

*Short Note*A Combined Earthquake–Landslide Source Model for the Tsunami from the 27 November 1945 M_w 8.1 Makran Earthquake

by Mohammad Heidarzadeh* and Kenji Satake

Abstract The tsunami of 27 November 1945 from an M_w 8.1 earthquake in the Makran subduction zone is the only instrumentally recorded and deadly tsunami in the northwest Indian Ocean; offshore Iran, Pakistan, Oman, and India. Despite the fact that some source models have been proposed based on seismic or far-field tsunami data, none of them was able to reproduce one important observation: near-field runup of 10–12 m. Here, we applied numerical modeling and examined three possible secondary sources: (1) splay faulting, (2) delayed rupture of the earthquake source, and (3) submarine landslides. These secondary sources were added to the existing state-of-the-art earthquake source for this tsunami. Results of simulations revealed that only a submarine landslide with dimensions of 15 km (length) \times 15 km (width), a thickness of 600 m, a volume of ~ 40 km³, and located at 63.0° E, 24.8° N is capable of reproducing the near-field tsunami observation. Such a combined earthquake–landslide source is consistent with all available observations including far-field tsunami waveforms in Karachi (Pakistan) and Mumbai (India), with near-field runup height of 10–12 m, coastal coseismic deformation data in Pasni (subsidence) and Ormara (uplift ~ 1 –3 m), and earthquake magnitude (M 8.0–8.3).

Electronic Supplement: Tables listing parameters of the splay fault and landslide scenarios, and figures showing deformation and coastal tsunami amplitudes from splay fault and landslide scenarios.

Introduction

The Makran subduction zone (MSZ) at the northwestern Indian Ocean (Fig. 1) has been at the center of attention in terms of earthquake and tsunami-hazard assessment in the aftermath of the large 2004 Sumatra–Andaman tsunami (e.g., Heidarzadeh, Pirooz, Zaker, Yalciner, *et al.*, 2008; Okal and Synolakis, 2008; Fritz *et al.*, 2010; Neetu *et al.*, 2011; Shah-Hosseini *et al.*, 2011; Smith *et al.*, 2012; Hoffmann *et al.*, 2013; Rajendran *et al.*, 2013; Kakar *et al.*, 2014; Okal *et al.*, 2015; Frohling and Szeliga, 2016; Schneider *et al.*, 2016). The MSZ, which is the result of subduction of the Arabian plate beneath the Eurasian plate at the rate of 19.5 mm/yr (Vernant *et al.*, 2004), has produced at least 13 $M \geq 6.5$ earthquakes (Fig. 1; Heidarzadeh, Pirooz, Zaker, Yalciner, *et al.*, 2008); among them is the M_w 8.1 earthquake on 27 November 1945 that was followed by a regional tsunami with at least 300 fatalities (Ambraseys and Melville, 1982; Okal and Synolakis,

2008). The Makran earthquake and tsunami of November 1945 is important for regional earthquake and tsunami hazard assessments because it is the largest recorded earthquake and tsunami in the region. Hence, it has been the basis for tsunami-hazard assessments for the coastal areas of Iran, Pakistan, India, and Oman (e.g., Heidarzadeh, Pirooz, Zaker, and Synolakis, 2008; Heidarzadeh, Pirooz, Zaker, and Yalciner, 2009; Rajendran *et al.*, 2013). The only other instrumentally recorded tsunami in the Makran region is the event of 23 September 2013, possibly generated by a submarine landslide that caused a maximum wave height of ~ 1 m with no damage (Heidarzadeh and Satake, 2014; Hoffmann *et al.*, 2014).

The available observations of the 1945 tsunami are (1) two tide gauge records in Karachi and Mumbai (Fig. 1d,e), which both can be considered as far-field records; (2) coastal deformation data including uplift of 1–3 m in Ormara (Pakistan) and subsidence in Pasni (Pakistan) (Page *et al.*, 1979); (3) magnitude of the earthquake in the 8.0–8.3 range (Byrne *et al.*, 1992); and (4) large near-field runup

*Now at Department of Mechanical, Aerospace, and Civil Engineering, Brunel University London, London, United Kingdom.

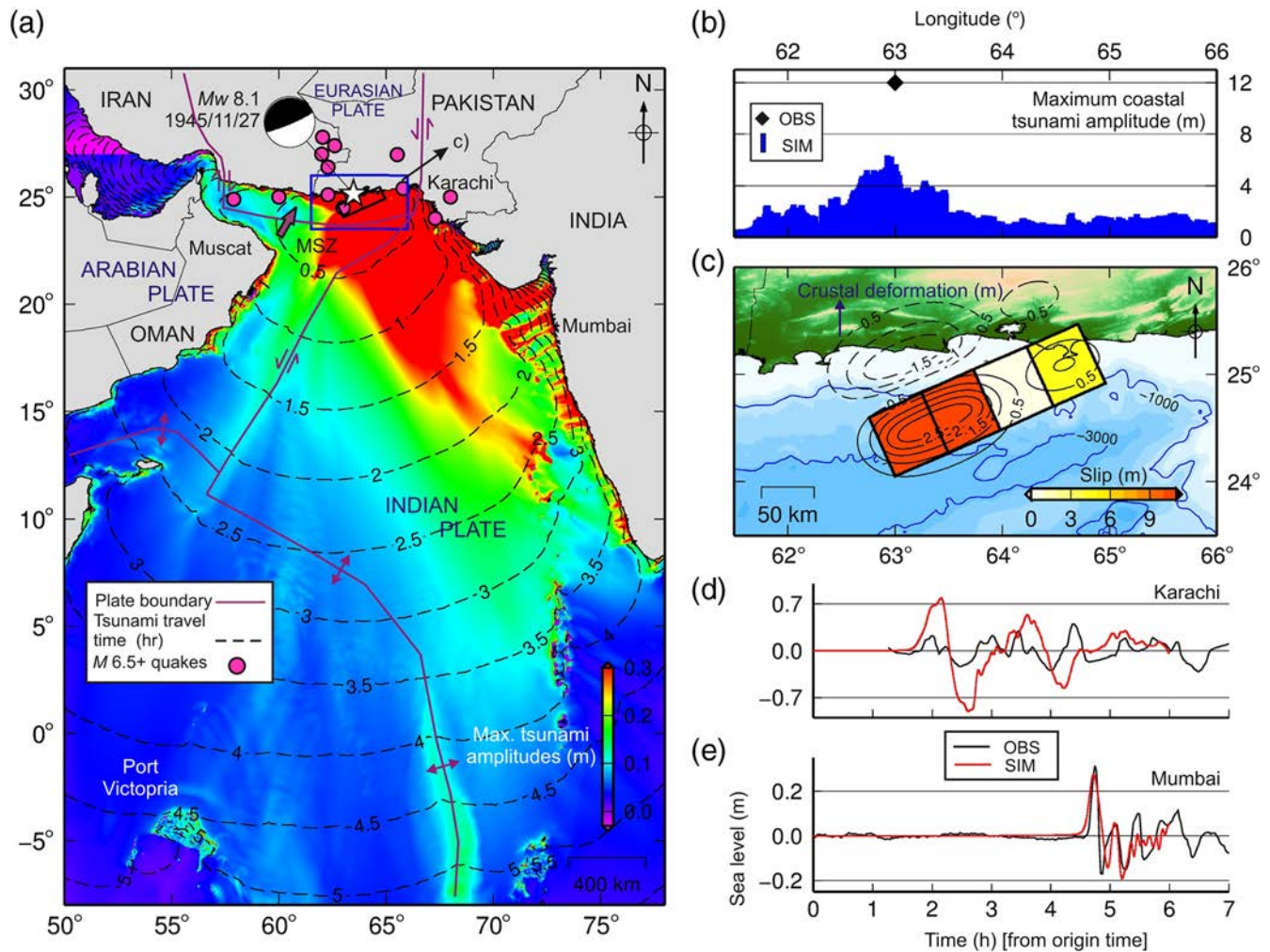


Figure 1. (a) Near- and far-field propagation of the Makran tsunami of 1945 resulted from the source proposed by Heidarzadeh and Satake (2015a). (b) Maximum simulated coastal wave amplitudes resulted from the source by Heidarzadeh and Satake (2015a). (c) The source model proposed by Heidarzadeh and Satake (2015a). (d) and (e) Comparison of observed (OBS) and simulated (SIM) waveforms at Karachi and Mumbai. The color version of this figure is available only in the electronic edition.

height of 10–12 m in a limited segment of the coast reported by Pendse (1946) and Ambraseys and Melville (1982). Despite the importance of the November 1945 Makran earthquake and tsunami, still no source model can explain all of the existing observations, though several source models have been proposed (e.g., Heidarzadeh, Pirooz, and Zaker, 2009; Heidarzadeh, Pirooz, Zaker, and Yalciner, 2009; Jaiswal *et al.*, 2009; Neetu *et al.*, 2011; Heidarzadeh and Satake, 2015a). The available source models have fault lengths of 100–200 km range, fault width of 70–100 km, slip values of 6.6–15 m, dip angles of 5.5°–15°, and are located at different locations from onshore area (e.g., Neetu *et al.*, 2011) to offshore region (e.g., Heidarzadeh, Pirooz, and Zaker, 2009; Heidarzadeh, Pirooz, Zaker, and Yalciner, 2009). Neetu *et al.* (2011) presented two observed tide gauge records of the 1945 tsunami for the first time, and their simulations resulted in an unsatisfactory match with the two observed tide gauge waveforms. By performing detailed simulations including runup calculations on dry land, Heidarzadeh, Pirooz, and Zaker (2009) reported a maximum

runup value of ~5 m. The two observed waveforms were unavailable at the time of the studies by Heidarzadeh, Pirooz, Zaker, and Yalciner (2009) and Jaiswal *et al.* (2009).

In a recent study, Heidarzadeh and Satake (2015a; hereafter, HS-2015) used items (1)–(3) among the above observations and developed a four-subfault source model (length of each subfault, 55 km; Fig. 1c). Comparison of coastal tsunami heights (Fig. 1b) showed that the maximum simulated tsunami amplitude is ~6 m; that is far less than the observed tsunami runup of 10–12 m. In their simulations, tsunami runups were estimated as the wave amplitudes on the coastal vertical wall that is an acceptable method for runup estimation (e.g., Tinti *et al.*, 2006). This large near-field observed runup, which appears disproportionate to the size of the earthquake (as a rule of thumb, tsunami runup heights are close to fault slip values; Okal and Synolakis, 2004), is possibly a result of secondary tsunami sources, such as submarine landslides triggered by the mainshock or splay faults branching from the plate boundary fault. Observations from

past tsunamis have shown that secondary sources were most likely responsible for large near-field runups. Examples are the 1998 Papua New Guinea tsunami from the secondary landslide source (Tappin *et al.*, 2001) and the 1964 Alaskan tsunami from the secondary splay fault (Plafker, 1972). Here, we explore the possible sources for this large near-field runup height during the 1945 Makran tsunami; then, we propose a comprehensive source model that is consistent with all available observations.

Possible Causes of Large Near-Field Runups

In general, three secondary sources might have contributed to such large near-field tsunami heights: (1) splay faults that may branch from the plate boundary during large inter-plate earthquakes; (2) delayed rupture of the seismic faults; and (3) submarine mass failures.

Splay Faults

As defined by Plafker (1972), splay faults are those with steep dip angles that branch in the upper plate from the plate boundary. The MSZ incorporates many splay faults, as shown in seismic profiles of the region by Mokhtari (2014) and Smith *et al.* (2012). According to Plafker (1972) and Heidarzadeh, Pirooz, and Zaker (2009), such splay faults can produce local large seafloor deformations that locally intensify the coastal tsunami heights. Evidence for splay faulting was presented for the 1964 Alaskan (Plafker, 1972), the San Andreas fault (Ando *et al.*, 2009), and the 1946 Nankai earthquakes (Cummins and Kaneda, 2000; Baba *et al.*, 2006; Moore *et al.*, 2007). Splay faults are characterized by relatively short length (~20–40 km), steep dip angles (i.e., ~20°–30°), and large slips (up to 10–15 m) (Plafker, 1972).

Delayed Rupture of the Seismic Faults

For tsunami modeling, the seafloor deformation is usually assumed to occur instantaneously, and the seismic rupture propagation and the duration time of seafloor rupture are usually neglected. This rupture time varies from around a minute for M 8 typical earthquakes to around 2–3 min for M 9 ones. An example of tsunami simulations by considering different rupture times for subfaults was conducted by Satake *et al.* (2013) for the case of the 2011 Tohoku tsunami. Satake *et al.* (2013) showed that the large offset (~100 km) between the location of the largest observed tsunami heights and the location of the largest fault slip can be explained by taking into account the rupture time of ~3 min.

Submarine Landslides

The MSZ has the largest accretionary wedge on the Earth, with a sediment thickness of ~7 km (Koppa *et al.*, 2000; Kukowski *et al.*, 2001). Such thick sediments may cause submarine mass failures in the form of landslides or

slumps that can produce large tsunami heights in the near field as evidenced during the 17 July 1998 Papua New Guinea tsunami (e.g., Synolakis *et al.*, 2002; Satake and Tanioka, 2003; Heidarzadeh and Satake, 2015b). Evidence for previous submarine mass failures in the MSZ was provided through bathymetric surveys (Kukowski *et al.*, 2001; Bourget *et al.*, 2010). Kukowski *et al.* (2001) identified a large regional landslide in the transition from midslope to the upper slope at around longitude of 63° E. Tsunami amplitudes from submarine landslide sources are mostly affected by dimensions of the sliding mass (length, width, and thickness), water depth, and travel distance of the landslide.

Methodology

Our method was based on adding a secondary source to the HS-2015 source, simulating the resulting tsunami from such a combined source, and comparing the near-field runup heights and observed waveforms in Karachi and Mumbai with those of simulations. Tsunami simulations were performed applying the TUNAMI-N2 model (Goto *et al.*, 1997; Yalciner *et al.*, 2004) that solves nonlinear shallow-water equations using a finite-difference method. The 30 arc-sec bathymetry data (equivalent to a 925 m × 925 m grid) from General Bathymetric Charts of the Oceans (GEBCO)-2014 digital atlas (Intergovernmental Oceanographic Commission [IOC] *et al.*, 2014) were used for tsunami modeling. Time step was 1.0 s in our nonlinear simulations. The simulated waveforms in Karachi and Mumbai are compared with the observations. The waveforms from the combined source should be similar to those from the HS-2015 source because these two stations are located in the far field, and any wave from a confined secondary source is unlikely to reach them. Our main objective was to reproduce large near-field runup heights of 10–12 m. Inundation on dry land was not included in our simulation because the precise location of observed runup and high-resolution topography are not available; instead, tsunami amplitudes on the coast were calculated that provide estimates of tsunami runup heights. We recorded the time history of the wave oscillations on the coastal vertical wall; then, the maximum value at each coastal point was used as an estimator of runup height at that particular point (e.g., Tinti *et al.*, 2006). This method is not affected by coseismic deformation (subsidence/uplift) because this method records tsunami amplitudes from normal sea-level elevation on the original bathymetry grid.

For modeling splay faults, a steep dip angle of 30° and large slip values of up to 25 m were used. We examined 12 splay fault scenarios with different fault parameters such as fault length and width (20–40 km), fault slip (9–25 m), strike angle (246°–270°) (Ⓔ Table S1, available in the electronic supplement to this article), and various locations (Ⓔ Fig. S1). Coseismic crustal deformation was calculated using the analytical formula of Okada (1985). The splay fault sources were added to the HS-2015 source. For all splay fault scenarios, the total moment magnitude (M_w) of the main earthquake source

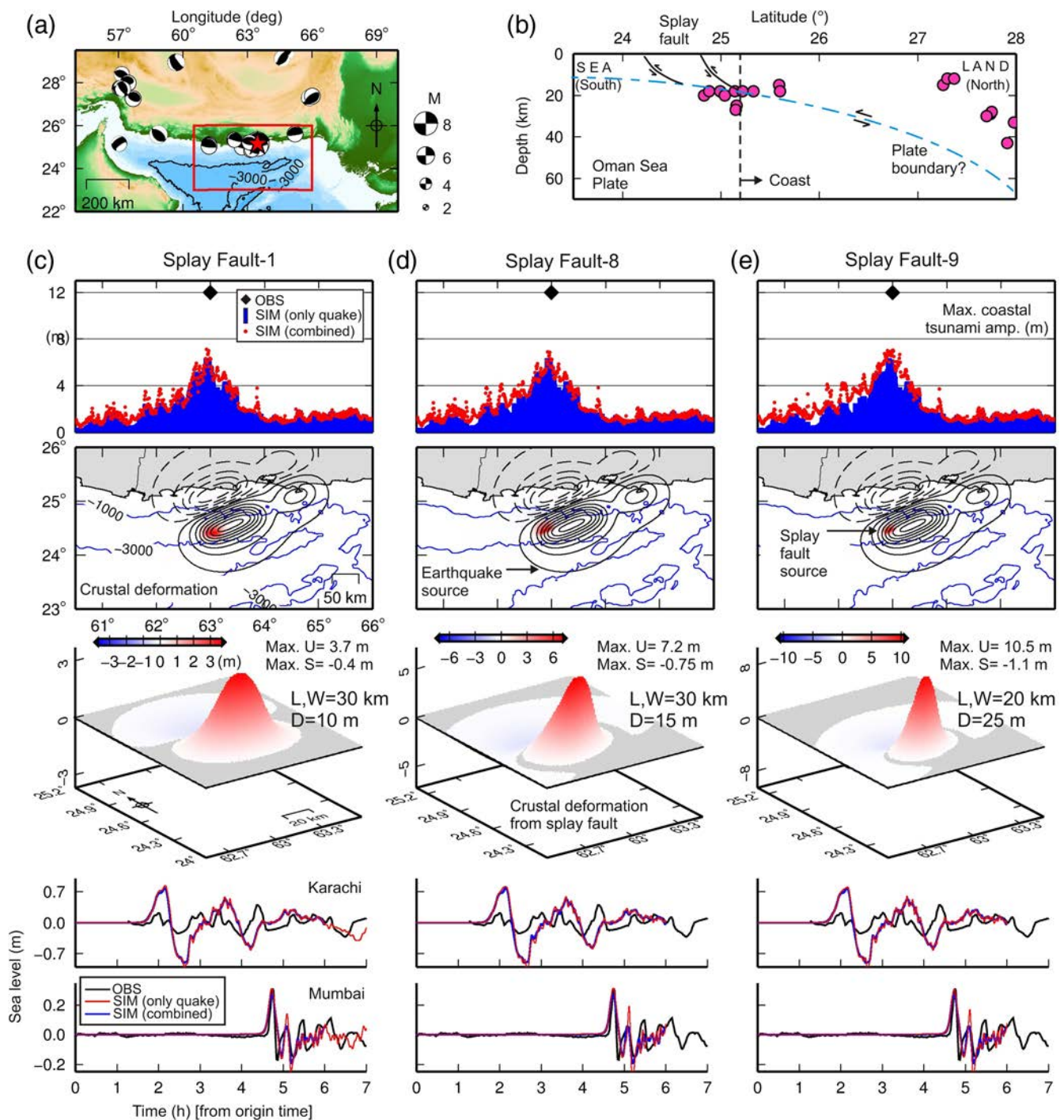


Figure 2. (a) Thrust fault earthquakes in the Makran subduction zone (MSZ). Data are from Global Centroid Moment Tensor (CMT) and Byrne *et al.* (1992). (b) A rough approximation of the MSZ plate boundary showing the depths of the thrust earthquakes. (c)–(e) Examples of results for splay fault scenarios showing three scenarios of 1, 8, and 9. Details of all 12 splay fault scenarios are shown in Table S1 (available in the electronic supplement to this article). For each case, coastal tsunami amplitudes, crustal deformation, 3D plot of the crustal deformation from the splay fault, and the simulated waveforms at Karachi and Mumbai are shown. U, uplift; S, subsidence; L, length; W, width; and D, displacement of the splay fault. The color version of this figure is available only in the electronic edition.

and the splay fault was kept below 8.3 because the M_w of the 1945 Makran earthquake was reported in the 8.0–8.3 range. For example, for the case of a splay fault with the length and width of 40 km, the slip of the splay fault was considered to be

9 m in order to maintain the total moment magnitude below 8.3 (scenario 3 in Table S1).

To consider the effects of delayed rupture on tsunami amplitudes, we assumed that different subfaults rupture at

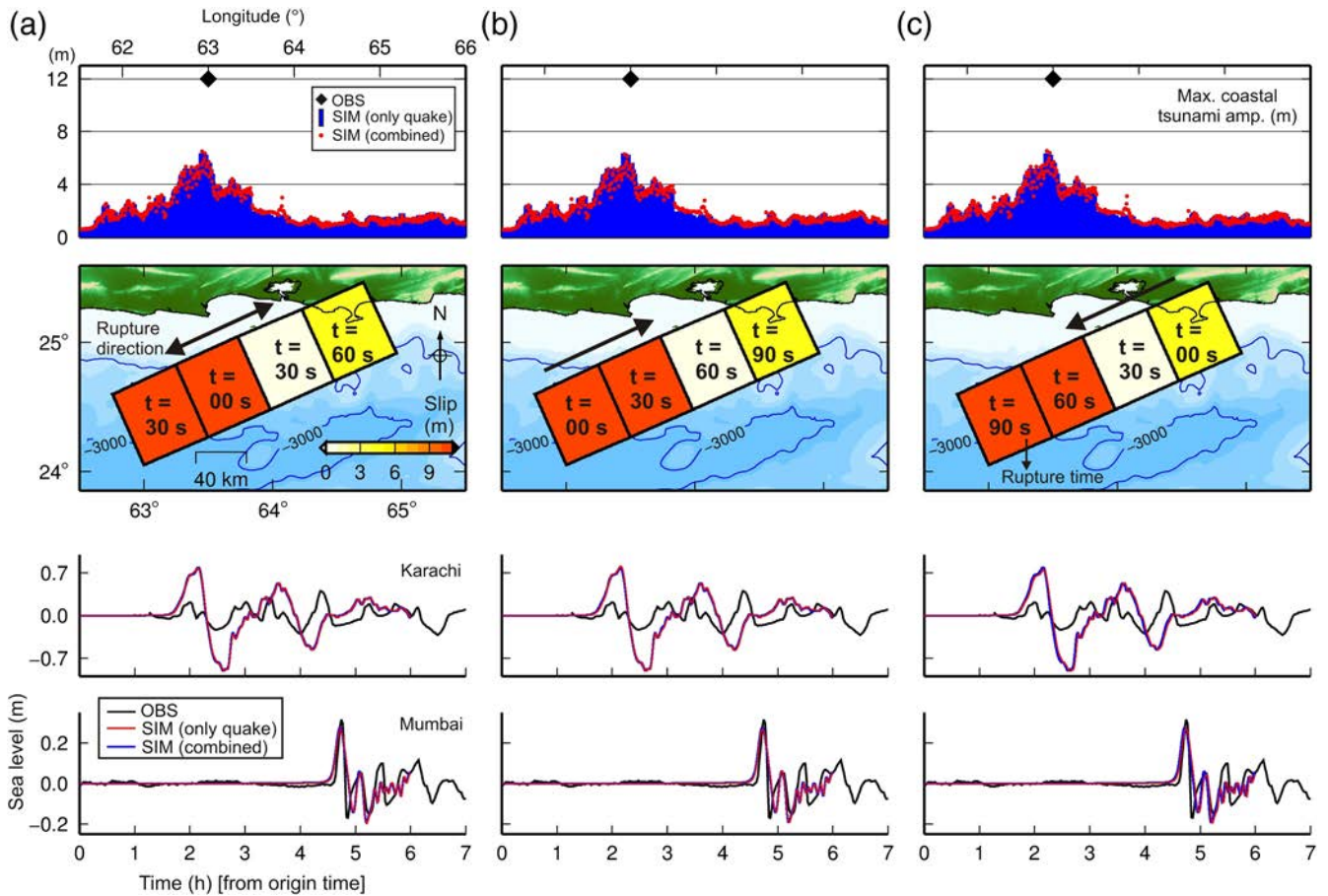


Figure 3. Effects of delays in rupture on coastal tsunami amplitudes. Three different patterns of (a) bilateral rupture, (b) rupture from south to north, and (c) rupture from north to south are examined here. For each case, coastal tsunami amplitudes and the simulated waveforms at Karachi and Mumbai are shown. The color version of this figure is available only in the electronic edition.

different times. By assuming a rupture velocity of 2 km/s, it takes ~ 30 s for a 55 km subfault to fully rupture. Three rupture directions were considered: bilateral, from south to north, and from north to south.

Landslide sources were modeled using semiempirical equations of Watts *et al.* (2005) to estimate the 3D initial sea surface shape (e.g., Synolakis *et al.*, 2002; Okal and Synolakis, 2004; Heidarzadeh *et al.*, 2014). Bulk density of the sliding material was assumed as 2150 kg/m^3 . We examined 12 landslide sources having various parameters, such as length and width (15–30 km), thickness (200–800 m), different locations with water depths of 1300–2000 m, and travel distance (1000–2000 m) (Table S2 and Fig. S3). The landslide sources were simultaneously added to the HS-2015 source.

Results

Figure 2 and Figure S2 present the results of adding a splay fault to the HS-2015 source. For all 12 scenarios of splay faults, the combined source was incapable of reproducing large near-field runup heights of 10–12 m (Fig. 2 and Figure S2). Despite using extremely large slip values of 25 m located very close to the shoreline, the coastal amplitudes

remain far below the observations (scenarios 11 and 12 in Figures S1 and S2). For scenarios 4 and 5, simulated coastal amplitudes from the combined source were noticeably larger than that of HS-2015 but smaller than observations. We changed the locations of these scenarios in order to examine whether they could reproduce the observations (scenarios 7, 8, 11, and 10 in Figures S1 and S2), but without success.

Figure 3 shows the results of simulations for three scenarios of delays in rupture, by considering up to 1.5 min of rupture duration and three different rupture directions. They showed that all three scenarios give similar results to that from HS-2015 (Fig. 3).

Figure 4 and Figure S4 show the results for 12 landslide scenarios as secondary sources. Out of these 12 scenarios, 6 of them were capable of reproducing large near-field coastal amplitudes. However, the maximum amplitudes were larger than the observations for some scenarios (e.g., scenarios 8–11 in Figure S4) or the large-amplitude segment of the coast was longer than that typically expected from a landslide source (e.g., scenarios 7 and 8 in Figure S4). By examining various scenarios, we reached scenario 12 (Fig. 4c), which satisfied all conditions. It gave 10–12 m of near-field coastal amplitudes; the large-amplitude segment of the coast was limited

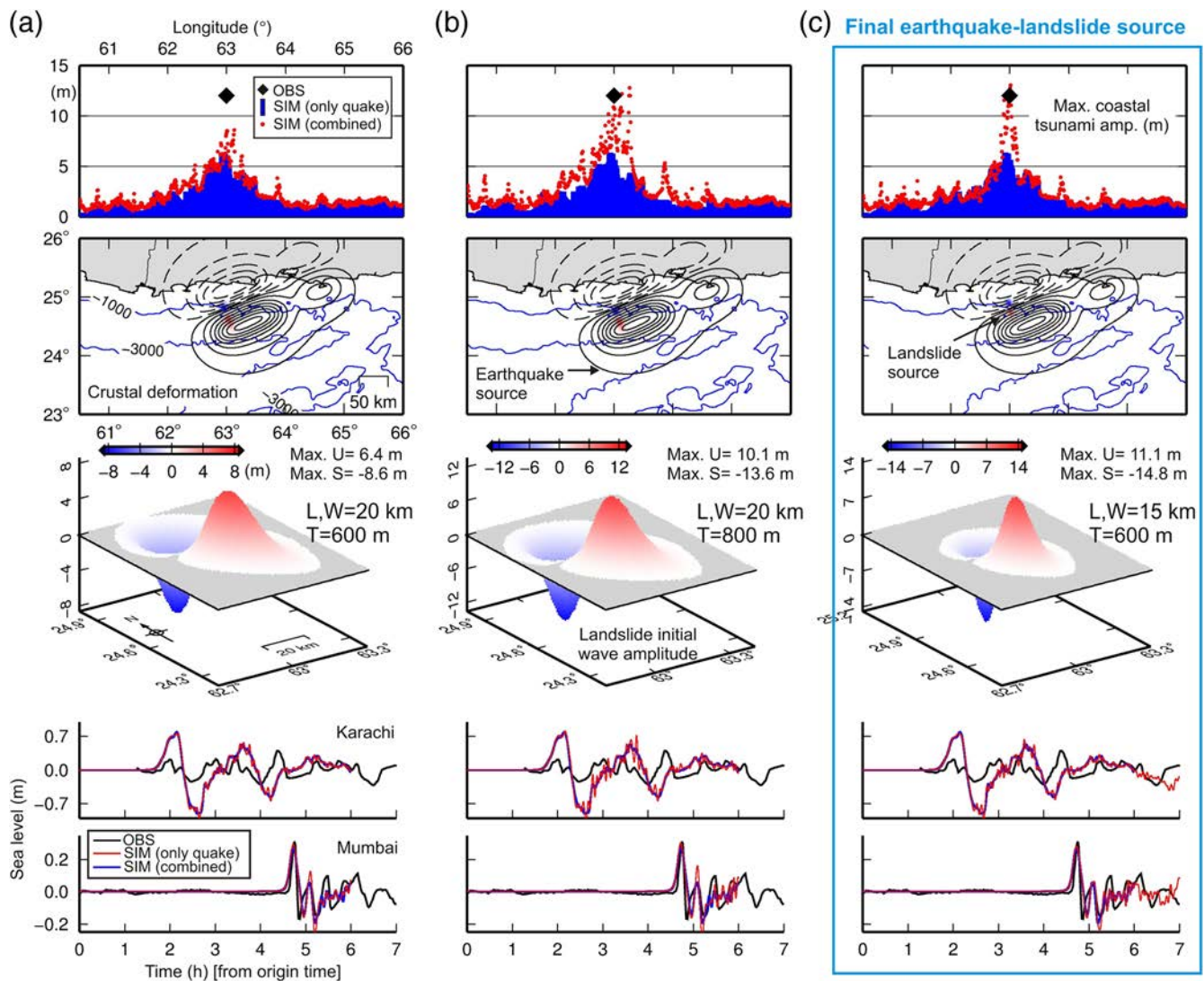


Figure 4. Results of landslide scenarios on the coastal tsunami amplitudes and far-field tide gauge records. Landslide scenarios (a) 6, (b) 7, and (c) 12 are shown here. The details of all 12 landslide scenarios are shown in Table S2. For each case, coastal tsunami amplitudes, crustal deformation from earthquake source and sea surface elevation from landslide source, 3D plot of the sea surface elevation from landslide source, and the simulated waveforms at Karachi and Mumbai are shown. U, uplift; S, subsidence; L, length; W, width; and T, landslide thickness. The color version of this figure is available only in the electronic edition.

(~20 km) and the simulated waveforms from the combined source were similar to that of HS-2015 (Fig. 4c). Our final landslide secondary source has a length and width of 15 km, a thickness of 600 m, and is located at 63.0° E and 24.8° N. This landslide has a volume of ~40 km³ (calculated using equation 2 of Enet and Grilli, 2007) and is located around the same site that a regional landslide was previously reported by Kukowski *et al.* (2001). However, we cannot confirm whether our hypothetical landslide is the same as that reported by Kukowski *et al.* (2001) or not because they did not report the age and volume of the slide.

Discussion

In addition to three possible secondary sources considered in this study, nonuniform slip distribution on the fault

plane also could be regarded as a potential source of large near-field runups. However, it does not seem to play a role for the 1945 Makran tsunami because both nonuniform slip (e.g., Heidarzadeh and Satake, 2015a) and uniform slip models (e.g., Heidarzadeh, Pirooz, and Zaker, 2009) resulted in the same runup heights of ~5–6 m.

Incapability of splay fault scenarios to reproduce large near-field runup can be attributed to the different initial sea surface wavefield generated from seismic (splay faults) and landslide sources. According to Figure 2 and Figure S1, the initial sea surface profile from splay faults is almost monopole (pure uplift), whereas it is dipole for submarine landslides (Fig. 4 and Figure S3). According to Heidarzadeh, Pirooz, and Zaker (2009), in order to reproduce large near-field runup of 10–12 m using splay faulting, the length of the splay fault needs to be ~100 km, and the parent earthquake

needs to have a moment magnitude of 8.6. This is far larger than the November 1945 Makran earthquake for which magnitude was in the domain of 8.0–8.3. In addition, the offshore Makran region has large potential for submarine mass failures triggered by seismic activities. For example, an inland M_w 7.7 earthquake in Pakistan triggered a small tsunami in the Makran region that was attributed to a submarine landslide (Heidarzadeh and Satake, 2014).

Characteristics of the final combined earthquake–landslide source model proposed here for the 1945 Makran tsunami (Fig. 4c) appear to be similar to those of the 1998 Papua New Guinea tsunami for which the source was a combination of earthquake and landslide sources (Geist, 2000; Tappin *et al.*, 2001; Lynett *et al.*, 2003; Satake and Tanioka, 2003; Heidarzadeh and Satake, 2015b): the segment of the coast with a large tsunami was ~20 km for both the 1998 Papua New Guinea and the 1945 MSZ events, and the waves from the landslide part of the source were not recorded on the far-field tide gauges for both events.

Conclusions

We examined three possible secondary sources (splay faulting, delayed ruptures, and submarine landslides) to explain the large near-field runup height of 10–12 m during the 1945 Makran tsunami. Among the aforesaid secondary sources, only a submarine landslide was capable of reproducing such large near-field runup. We propose a submarine landslide with a length and width of 15 km, a thickness of 600 m, a volume of ~40 km³, and located at 63.0° E and 24.8° N as the secondary source to be added to the earthquake source of Heidarzadeh and Satake (2015a) for this event. Such a combined earthquake–landslide source is consistent with all available instrumental and historical records of this tsunami.

Data and Resources

We used the 30 arcsec bathymetry data from General Bathymetric Charts of the Oceans (GEBCO)-2014 digital atlas for tsunami modeling which is provided by Intergovernmental Oceanographic Commission (IOC) *et al.* (2014). Two tide gauge records of the 1945 Makran tsunami were digitized from Neetu *et al.* (2011). Focal mechanisms of the thrust earthquakes in the Makran subduction zone (MSZ) are from Byrne *et al.* (1992) and also from the Global Centroid Moment Tensor (CMT) Project (<http://www.globalcmt.org/>, last accessed November 2015). The earthquake source model of the 1945 Makran tsunami is from Heidarzadeh and Satake (2015a).

Acknowledgments

Most of the figures were drafted using the Generic Mapping Tool (GMT) software (Wessel and Smith, 1998). We thank Takeo Ishibe (Association for the Development of Earthquake Prediction, Tokyo, Japan) and Tomoya Harada (Earthquake Research Institute [ERI], University of Tokyo) for their assistance in seismicity analysis of the Makran subduction zone. We are grateful to Associate Editor Mark W. Stirling and two anonymous reviewers for their constructive review comments.

References

- Ambraseys, N. N., and C. P. Melville (1982). *A History of Persian Earthquakes*, Cambridge University Press, Cambridge, United Kingdom, 219 pp.
- Ando, R., B. E. Shaw, and C. H. Scholz (2009). Quantifying natural fault geometry: Statistics of splay fault angles, *Bull. Seismol. Soc. Am.* **99**, no. 1, 389–395.
- Baba, T., P. R. Cummins, T. Hori, and Y. Kaneda (2006). High precision slip distribution of the 1944 Tonankai earthquake inferred from tsunami waveforms: Possible slip on a splay fault, *Tectonophysics* **426**, no. 1, 119–134.
- Bourget, J., S. Zaragosi, S. Ellouz-Zimmermann, E. Ducassou, M. A. Prins, T. Garlan, V. Lanfumey, J. L. Schneider, P. Rouillard, and J. Giraudeau (2010). Highstand vs. lowstand turbidite system growth in the Makran active margin: Imprints of high-frequency external controls on sediment delivery mechanisms to deep water systems, *Mar. Geol.* **274**, no. 1, 187–208.
- Byrne, D. E., L. R. Sykes, and D. M. Davis (1992). Great thrust earthquakes and aseismic slip along the plate boundary of the Makran subduction zone, *J. Geophys. Res.* **97**, 449–478.
- Cummins, P. R., and Y. Kaneda (2000). Possible splay fault slip during the 1946 Nankai earthquake, *Geophys. Res. Lett.* **27**, no. 17, 2725–2728.
- Enet, F., and S. T. Grilli (2007). Experimental study of tsunami generation by three-dimensional rigid underwater landslides, *J. Waterw. Port Coast. Ocean Eng.* **133**, 442–454.
- Fritz, H. M., C. D. Blount, F. B. Albusaidi, and A. H. M. Al-Harthy (2010). Cyclone Gonu storm surge in Oman, *Estuar. Coast. Shelf Sci.* **86**, 102–106.
- Frohling, E., and W. Szeliga (2016). GPS constraints on interplate locking within the Makran subduction zone, *Geophys. J. Int.* **205**, no. 1, 67–76.
- Geist, E. L. (2000). Origin of the 17 July 1998 Papua New Guinea tsunami: Earthquake or landslide, *Seismol. Res. Lett.* **71**, no. 3, 344–351.
- Goto, C., Y. Ogawa, N. Shuto, and F. Imamura (1997). *Numerical Method of Tsunami Simulation with the Leap-Frog Scheme (IUGG/IOC Time Project)*, IOC Manual, UNESCO, no. 35.
- Heidarzadeh, M., and K. Satake (2014). Possible sources of the tsunami observed in the northwestern Indian Ocean following the 2013 September 24 M_w 7.7 Pakistan inland earthquake, *Geophys. J. Int.* **199**, 752–766.
- Heidarzadeh, M., and K. Satake (2015a). New insights into the source of the Makran tsunami of 27 November 1945 from tsunami waveforms and coastal deformation data, *Pure Appl. Geophys.* **172**, nos. 3/4, 621–640.
- Heidarzadeh, M., and K. Satake (2015b). Source properties of the 1998 July 17 Papua New Guinea tsunami based on tide gauge records, *Geophys. J. Int.* **202**, no. 1, 361–369.
- Heidarzadeh, M., S. Krastel, and A. C. Yalciner (2014). The state-of-the-art numerical models for modeling landslide tsunamis: A short review, in *Submarine Mass Movements and Their Consequences*, Sixth Ed., S. Krastel (Editor), Springer, London, United Kingdom, 483–495.
- Heidarzadeh, M., M. D. Pirooz, and N. H. Zaker (2009). Modeling the near-field effects of the worst-case tsunami in the Makran subduction zone, *Ocean Eng.* **36**, 368–376.
- Heidarzadeh, M., M. D. Pirooz, N. H. Zaker, and C. E. Synolakis (2008). Evaluating tsunami hazard in the northwestern Indian Ocean, *Pure Appl. Geophys.* **165**, 2045–2058.
- Heidarzadeh, M., M. D. Pirooz, N. H. Zaker, and A. C. Yalciner (2009). Preliminary estimation of the tsunami hazards associated with the Makran subduction zone at the northwestern Indian Ocean, *Nat. Hazards* **48**, 229–243.
- Heidarzadeh, M., M. D. Pirooz, N. H. Zaker, A. C. Yalciner, M. Mokhtari, and A. Esmaeily (2008). Historical tsunami in the Makran subduction zone off the southern coasts of Iran and Pakistan and results of numerical modeling, *Ocean Eng.* **35**, 774–786.
- Hoffmann, G., S. Al-Yahyai, G. Naem, M. Kociok, and C. Grützner (2014). An Indian Ocean tsunami triggered remotely by an onshore earthquake in Balochistan, Pakistan, *Geology* **42**, no. 10, 883–886.

- Hoffmann, G., N. Rupprechter, N. Albalushi, C. Grutzner, and K. Reicherter (2013). The impact of the 1945 Makran tsunami along the coastlines of the Arabian Sea (northern Indian Ocean)—A review, *Zeitschrift für Geomorphologie* **57**, 257–277.
- Intergovernmental Oceanographic Commission (IOC), International Hydrographic Organization (IHO) and British Oceanographic Data Centre (BODC) (2014). *Centenary Edition of the GEBCO Digital Atlas*, published on CD-ROM on behalf of the Intergovernmental Oceanographic Commission and the International Hydrographic Organization as part of the General Bathymetric Chart of the Oceans, British Oceanographic Data Centre, Liverpool, United Kingdom.
- Jaiswal, R. K., A. P. Singh, and B. K. Rastogi (2009). Simulation of the Arabian Sea tsunami propagation generated due to 1945 Makran earthquake and its effect on western parts of Gujarat (India), *Nat. Hazards* **48**, 245–258.
- Kakar, D. M., G. Naeem, A. Usman, H. Hasan, H. A. Lohdi, S. Srinivasalu, V. Andrade, C. P. Rajendran, A. N. Beni, M. A. Hamzeh, *et al.* (2014). Elders recall an earlier tsunami on Indian Ocean shores, *Eos Trans. AGU* **95**, no. 51, 485–486.
- Koppa, C., J. Fruehn, E. R. Flueh, C. Reichert, N. Kukowski, J. Bialas, and D. Klaeschen (2000). Structure of the Makran subduction zone from wide-angle and reflection seismic data, *Tectonophysics* **329**, 171–191.
- Kukowski, N., T. Schillhorn, K. Huhn, U. von Rad, S. Husen, and E. R. Flueh (2001). Morphotectonics and mechanics of the central Makran accretionary wedge off Pakistan, *Mar. Geol.* **173**, no. 1, 1–19.
- Lynett, P. J., J. C. Borrero, P. L.-F. Liu, and C. E. Synolakis (2003). Field survey and numerical simulations: A review of the 1998 Papua New Guinea tsunami, *Pure Appl. Geophys.* **160**, 2119–2146.
- Mokhtari, M. (2014). The role of splay faulting in increasing the devastation effect of tsunami hazard in Makran, Oman Sea, Arab, *J. Geosci.* **8**, no. 7, 4291–4298, doi: [10.1007/s12517-014-1375-1](https://doi.org/10.1007/s12517-014-1375-1).
- Moore, G. F., N. L. Bangs, A. Taira, S. Kuramoto, E. Pangborn, and H. J. Tobin (2007). Three-dimensional splay fault geometry and implications for tsunami generation, *Science* **318**, no. 5853, 1128–1131.
- Neetu, S., I. Suresh, R. Shankar, B. Nagarajan, R. Sharma, S. S. C. Shenoi, A. S. Unnikrishnan, and D. Sundar (2011). Trapped waves of the 27 November 1945 Makran tsunami: Observations and numerical modeling, *Nat. Hazards* **59**, 1609–1618.
- Okada, Y. (1985). Surface deformation due to shear and tensile faults in a half-space, *Bull. Seismol. Soc. Am.* **75**, 1135–1154.
- Okal, E. A., and C. E. Synolakis (2004). Source discriminants for near-field tsunamis, *Geophys. J. Int.* **158**, no. 3, 899–912.
- Okal, E. A., and C. E. Synolakis (2008). Far-field tsunami hazard from mega-thrust earthquakes in the Indian Ocean, *Geophys. J. Int.* **172**, 995–1015.
- Okal, E. A., H. M. Fritz, M. A. Hamzeh, and J. Ghasemzadeh (2015). Field survey of the 1945 Makran and 2004 Indian Ocean tsunamis in Baluchistan, Iran, *Pure Appl. Geophys.* **172**, no. 12, 3343–3356.
- Page, W. D., J. N. Alt, L. S. Cluff, and G. Plafker (1979). Evidence for the recurrence of large-magnitude earthquakes along the Makran coast of Iran and Pakistan, *Tectonophysics* **52**, no. 1, 533–547.
- Pendse, C. G. (1946). The Makran earthquake of the 28th November 1945, *India Meteorol. Depart. Sci. Notes* **10**, 141–145.
- Plafker, G. (1972). Alaskan earthquake of 1964 and Chilean earthquake of 1960: Implications for arc tectonics, *J. Geophys. Res.* **77**, 901–923.
- Rajendran, C. P., K. Rajendran, M. Shah-Hosseini, A. Naderi Beni, C. M. Nautiyal, and R. Andrews (2013). The hazard potential of the western segment of the Makran subduction zone, northern Arabian Sea, *Nat. Hazards* **65**, 219–239.
- Satake, K., and Y. Tanioka (2003). The July 1998 Papua New Guinea earthquake: Mechanism and quantification of unusual tsunami generation, *Pure Appl. Geophys.* **160**, nos. 10/11, 2087–2118.
- Satake, K., Y. Fujii, T. Harada, and Y. Namegaya (2013). Time and space distribution of coseismic slip of the 2011 Tohoku earthquake as inferred from tsunami waveform data, *Bull. Seismol. Soc. Am.* **103**, no. 2B, 1473–1492.
- Schneider, B., G. Hoffmann, and K. Reicherter (2016). Scenario-based tsunami risk assessment using a static flooding approach and high-resolution digital elevation data: An example from Muscat in Oman, *Global Planet. Change* **139**, 183–194.
- Shah-hosseini, M., C. Morhange, A. Naderi Beni, N. Marriner, H. Lahijani, M. Hamzeh, and F. Sabatier (2011). Coastal boulders as evidence for high-energy waves on the Iranian coast of Makran, *Mar. Geol.* **290**, 17–28.
- Smith, G., L. McNeill, T. J. Henstock, and J. Bull (2012). The structure and fault activity of the Makran accretionary prism, *J. Geophys. Res.* **117**, no. B7, doi: [10.1029/2012JB009312](https://doi.org/10.1029/2012JB009312).
- Synolakis, C. E., J.-P. Bardet, J. C. Borrero, H. L. Davies, E. A. Okal, E. A. Silver, S. Sweet, and D. R. Tappin (2002). The slump origin of the 1998 Papua New Guinea tsunami, *Proc. Math. Phys. Sci.* **458**, no. 2020, 763–789.
- Tappin, D. R., P. Watts, G. M. McMurtry, Y. Lafoy, and T. Matsumoto (2001). The Sissano, Papua New Guinea tsunamis of July 1998—Offshore evidence on the source mechanism, *Mar. Geol.* **175**, no. 1, 1–23.
- Tinti, S., A. Armigliato, A. Manucci, G. Pagnoni, F. Zaniboni, A. C. Yalciner, and Y. Altinok (2006). The generating mechanisms of the August 17, 1999 Izmit Bay (Turkey) tsunamis: Regional (tectonic) and local (mass instabilities) causes, *Mar. Geol.* **225**, 311–330.
- Vernant, Ph., F. Nilforoushan, D. Hatzfeld, M. R. Abbassi, C. Vigny, F. Masson, H. Nankali, J. Martinod, A. Ashtiani, R. Bayer, *et al.* (2004). Present-day crustal deformation and plate kinematics in the Middle East constrained by GPS measurements in Iran and northern Oman, *Geophys. J. Int.* **157**, 381–398.
- Watts, P., S. T. Grilli, D. Tappin, and G. J. Fryer (2005). Tsunami generation by submarine mass failure. II: Predictive equations and case studies, *J. Waterw. Port Coast. Ocean Eng.* **131**, no. 6, 298–310.
- Wessel, P., and W. H. F. Smith (1998). New, improved version of Generic Mapping Tools released, *Eos Trans. AGU* **79**, no. 47, 579.
- Yalciner, A. C., E. Pelinovsky, T. Talipova, A. Kurkin, A. Kozelkov, and A. Zaitsev (2004). Tsunamis in the Black Sea: Comparison of the historical, instrumental, and numerical data, *J. Geophys. Res.* **109**, no. 12, 2003–2113.

Port and Airport Research Institute (PARI)
3-1-1 Nagase, Yokosuka
Kanagawa 239-0826, Japan
heidarzadeh@pari.go.jp
(M.H.)

Earthquake Research Institute
The University of Tokyo
1-1-1 Yayoi, Bunkyo-ku
Tokyo 113-0032, Japan
satake@eri.u-tokyo.ac.jp
(K.S.)

Manuscript received 21 June 2016;
Published Online 3 January 2017